Macromolecules
ARTICLE

Macromolecules **2010**, *43*, 10071–10077 **10071**
DOI: 10.1021/ma101791m

Measurement and Analysis of the Angular Guided-Wave Depolarized Light Scattering Patterns from Block Copolymer Thin Films

Zhuangxi Fang,[†] Maurice C. Newstein,[†] Bruce A. Garetz,*[,†] and Nitash P. Balsara*[,‡]

[†]*Department of Chemical and Biological Sciences, Othmer-Jacobs Department of Chemical and Biological Engineering, and Department of Electrical and Computer Engineering, Polytechnic Institute of NYU, Six Metrotech Center, Brooklyn, New York 11201, United States, and* [‡]*Department of Chemical Engineering and Materials Sciences Division and Environmental Energy Technologies Division, Lawrence Berkeley National Laboratory, University of California, Berkeley, Berkeley, California 94720, United States*

Received August 5, 2010; Revised Manuscript Received October 27, 2010

ABSTRACT: We have measured and analyzed the angular scattering patterns in guided-wave depolarized light scattering (GWDLS) from 500 nm thick diblock copolymer thin films of poly(styrene-*block*-isoprene) using diffraction grating couplers. The measured pattern is decomposed into the sum of contributions from ordered grains and grating birefringence. Measured patterns are well fitted using a grain model consisting of disks lying in the film plane with elliptical cross sections, randomly oriented optic axes, and variable-length major axes.

Introduction

Block copolymers can self-organize into ordered nanoscale structures consisting of lamellae, cylinders, spheres, and gyroids.[1] When these structures are formed by a process of nucleation and growth, the resulting material consists of a collection of microscale regions in which the nanostructures are coherent (parallel and in-phase), referred to as "grains". In the case of lamellae and cylinders, these grains are optically anisotropic and exhibit form birefringence and depolarized light scattering (DPLS). Over the past two decades, our group and other researchers have shown how the analysis of depolarized scattering patterns can be used to characterize the size, shape, and growth kinetics of block copolymer grains in bulk samples.[2−6] Chastek and Lodge have shown how polarized light microscopy (POM) can be used to obtain similar information when the grain dimensions exceed several micrometers.[7−9]

Block copolymer thin films composed of dense periodic structures are expected to enable a wide variety of applications in modern nanotechnology.[10−13] Knowledge of the structural information and the phase-transformation kinetics of the lateral grains within the films is of particular interest in understanding the dynamics of microphase separation and is critical in the applications of these ordered systems. Two complementary categories of characterization methods have been used to study the ordered grain structures within thin-film samples. Position space techniques, such as atomic force microscopy (AFM), transmission electron microscopy (TEM), and scanning force microscopy (SFM), provide a direct view of the grain morphologies.[14−16] However, each image from microscopy methods represents only a very local part of the sample, and a large number of images are needed to obtain statistically significant quantitative information on the ordered grains. Complementing position space methods, reciprocal space techniques can quantify statistical properties of the sample in a single measurement. In this category, grazing incidence small-angle X-ray scattering (GISAXS),[17] grazing incidence wide-angle X-ray diffraction (GIWAXD),[18] resonant soft X-ray scattering (RSOXS),[19] and grazing incidence small-angle neutron scattering (GISANS)[20] are useful in studying the lateral order in thin-film samples, but they provide no structural information on the grains. Extending light scattering methods from bulk materials to thin films has been a challenging problem. Several years ago our group reported a method for obtaining light scattering information from a thin film by coupling a laser beam into the film, which acted as a planar waveguide. As the light propagated along the film it generated depolarized scattered light, which was then coupled out of the film and analyzed. To date, this method, called guided-wave depolarized light scattering (GWDLS), remains the only reciprocal space technique that quantifies the grain structures within ordered block copolymer thin films.[21−23]

In a GWDLS measurement, laser light is coupled into and out of the thin-film waveguide through optical coupling devices. The incident and scattered light propagate in either discrete transverse electric (TE) or transverse magnetic (TM) modes, which are orthogonal in polarization and can be isolated using an analyzing polarizer. Analysis of the depolarized scattered light reveals structural information on the optically anisotropic grains. GWDLS experiments have been conducted using two different coupling methods. Prism-coupled GWDLS was the first attempt at this technique, in which the absolute grain size was measured from the ratio of the integrated depolarized power to the integrated polarized power.[21,22] However, this coupling method is applicable only to hard films and cannot be used to study soft samples near the order−disorder transition temperature (T_{ODT}). Grating-coupled GWDLS was developed to overcome these shortcomings. The T_{ODT}'s of thin-film samples were measured using temperature-scanned GWDLS with diffraction grating couplers.[23] However, the grating couplers produced an artifactual depolarized signal owing to the form birefringence of the diffraction gratings. Because of the substantial magnitude of this artifact, the previous work using grating-coupled GWDLS was limited to the qualitative detection of the presence of the ordered state. DPLS studies of bulk block copolymer melts and solutions demonstrated that the angular scattered pattern contained detailed structural information on the grains.[5] In GWDLS, accurate measurement and analysis of the angular scattered pattern are challenging because of the form birefringence of the gratings.

*To whom correspondence should be addressed.

Published on Web 11/16/2010

In order to tackle the problem of the grating birefringence, the theoretical relationship of the birefringence and the grating profile was studied using a slicing method,[24] and the coupling efficiency was also calculated using a Green's function approach developed by Giallorenzi et al.[25] Calculations indicated that the birefringence from the grating couplers inevitably accompanied efficient coupling of the guided wave. Fortunately, the grating parameters could be optimally designed to minimize the birefringence amplitude while maintaining a high level of coupling efficiency.[24] With an optimally designed grating coupler, accurate measurement of the angular GWDLS pattern becomes feasible.

The main purpose of this paper is to report the first measurement and analysis of the angular GWDLS pattern from a block copolymer thin film. In the previous work on prism-coupled GWDLS, the quantitative relationship between the scattered field and the grain structure was derived based on a Green's function approach, and the integrated depolarized power ratio was calculated using a correlation method.[22] However, the calculation was based on a simple ideal grain model, and only one length scale could be determined. In this paper, an amplitude method with arbitrary grain shape model is applied to calculate the angular GWDLS pattern. With this theoretical result, the measured pattern can be decomposed into contributions from the ordered grains and the grating birefringence through a three-parameter fitting procedure, which allows the determination of additional quantitative information about the grain structure.

Experimental Section

Experiments described in this paper were performed primarily on an anionically synthesized poly(styrene-*block*-isoprene) copolymer. The molecular weights of the polystyrene and polyisoprene blocks were 7.3 and 22.6 kg/mol, respectively, and this polymer is referred to as SI(7−23). The volume fraction of the polystyrene block in SI(7−23) was 0.217, and the morphology in the ordered state was previously determined, through SAXS and TEM, to be hexagonally packed cylinders of polystyrene in a polyisoprene matrix.[26] The T_{ODT} was determined experimentally to be 98 °C by an optical birefringence measurement, in which the total power transmitted through a sample held between crossed polarizers is monitored as a function of increasing temperature. As the temperature rises above T_{ODT}, the sample birefringence vanishes, and the transmitted power drops to zero.[26]

Two diffraction gratings were etched by Ibsen Photonics in Farum, Denmark. A 1 mm × 1 mm input coupling grating and a 2 mm × 5 mm output coupling grating separated by 10 mm were etched into each 25 × 30 × 2 mm fused silica substrate. Each coupler had a grating period of 350 nm, a trench depth of 225 nm, and a trench width of 160−170 nm. Block copolymer thin film samples were spin-coated onto the rectangular substrates. After each use, the substrates were soaked in toluene overnight and then immersed for 20−30 min in a piranha solution, which was prepared from a 3:1 volume ratio of concentrated sulfuric acid and hydrogen peroxide, to remove remaining organic matter from the surface and the grating trenches. After piranha etching, substrates were removed from the piranha solution, rinsed with deionized water for 20 min, and then spin-dried at 2000 rpm for 1 min with the gratings placed face up. Substrates were rinsed again with toluene and spin-dried. Finally, an 8 wt % solution of SI(7−23) polymer dissolved in toluene was deposited onto the substrate and spin-coated at 2000 rpm for 1 min. The coated films were about 500 nm thick and supported only one TE and one TM waveguide mode. The samples were placed in a vacuum oven for 12 h to drive off the remaining solvent. After that, the temperature was raised to 103 °C for 20 min to erase the thermal history of the samples and was then kept at 93 °C for 2 h to develop the ordered structure. The substrate with the annealed thin-film sample was then clamped into the sample chamber for the GWDLS measurement.

The GWDLS apparatus is similar to the one presented in the previous paper except for the detection devices, as shown schematically in Figure 1a.[23] The red helium−neon laser source produced a linearly polarized beam of light with wavelength λ_0 = 632.8 nm. A half-wave retardation plate and a polarizer were used to adjust the polarization of the incident beam. The substrate with the thin-film sample was held in a sample chamber mounted on a rotational stage, equipped with a three-axis micrometer for precise rotational and translational control. The incident beam with 10 mW of power was coupled into the TE mode of the polymer film through the input grating coupler, as shown in Figure 1b. The optimal coupling condition was achieved through angular control from the rotational stage and translational control from the three-axis micrometer. Both the scattered TE and TM waves were then coupled out of the film through the output grating and separated through the analyzing polarizer. The scattered pattern was incident on a screen, which was a piece of Parafilm M sealing film held between two glass plates, and was then captured using a Dage-MTI CCD 72 camera with the room lights off. The distance between the output grating and the screen was 20 cm. In DPLS experiments on bulk samples, the imaging screen is a piece of white paper. In GWDLS, the opacity of white paper is too great to generate a detectable image with the CCD camera. The more translucent Parafilm scatters more light in the forward direction, overcoming this problem. (The Parafilm was tested for homogeneity and uniformity of thickness and was found to be superior to the white paper screens we had used previously. When the Parafilm was illuminated with a laser beam, the forward scattered intensity was constant over the 4 in. × 4 in. area of the screen, with a local deviation of ~3%, compared to a deviation of ~5% for a white paper screen.) After recording the scattered pattern, a ruler was placed at the same position as the screen, and an image was recorded with the room lights on, in order to determine the distance between the pixels and thus the scattering angle corresponding to each pixel. Typical captured polarized and depolarized patterns are shown in Figure 2. In the previous paper, it was proposed that capturing the angular pattern using a CCD camera

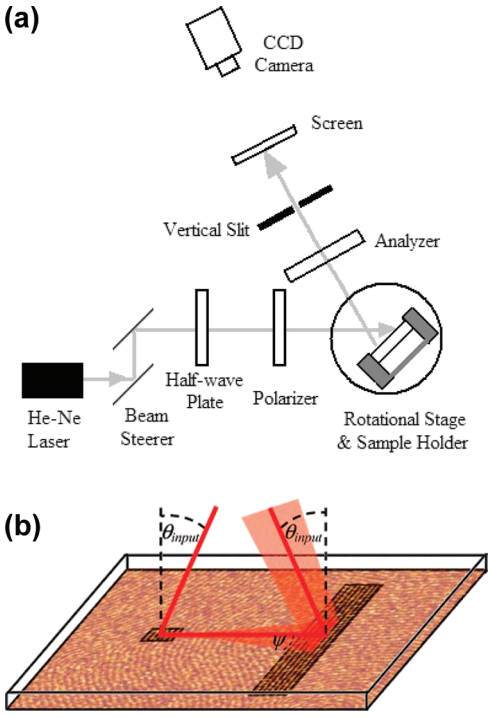

Figure 1. Schematic of the GWDLS apparatus: (a) overall layout of the optical components; (b) details of grating coupler geometry. Grating and film are on the bottom surface of the substrate. The red laser beam (left) enters the substrate through the uncoated surface and propagates through the substrate before encountering the input grating, which diffracts the beam into the TE mode of the film. Scattered light is coupled out through the output grating (right).

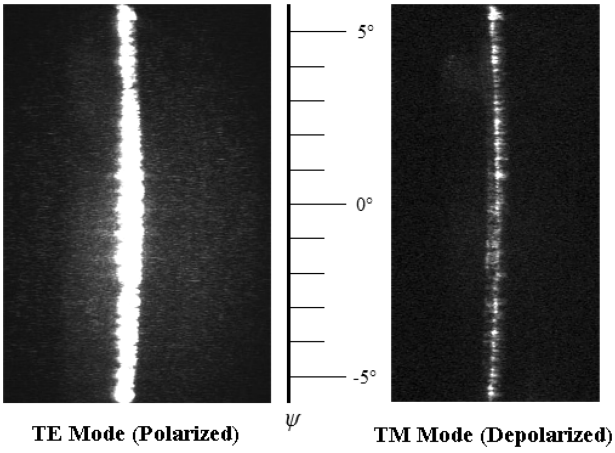

Figure 2. Angular GWDLS pattern captured by the CCD camera.

might allow direct angular separation of the depolarized contributions from the grains and the grating.[23] This turns out not to be the case because the transverse angular width of the *m*-lines exceeds the small difference (≤0.2°) between the TE and TM coupling angles. Fortunately, it is still possible to separate these contributions in the data processing step.

The CCD camera captures the relative but not the absolute light intensity. For theoretical fitting purposes, the depolarized intensity ratio in the forward direction was measured using a Coherent LabMaster E optical power meter as described in the previous paper,[23] so that the measured angular pattern can be rescaled accordingly.

Each captured image was digitized to be a 640 × 480 matrix consisting of integers ranging from 0 to 255, and the corresponding dark background was subtracted. In each row of the matrix, the elements near the center were averaged to obtain the intensity at the corresponding scattering angle. When capturing the patterns, the center of the image was adjusted to be close to the forward direction, which was precisely located at the row where the sum of the squared differences between the intensities at corresponding positive and negative angles was minimized. The pattern was further smoothed by averaging the intensities in every three rows on both sides and then rescaled using the measured central depolarized intensity ratio.

Theoretical Scattered Pattern from the Grains

The three-layer configuration and the laboratory coordinate system are depicted in Figure 3. The substrate, film, and air layers are labeled with subscripts 1, 2, and 3, respectively. In the previous theoretical work, it was shown that the scattered electric field at point **r** within the waveguide from a source point **r′** can be obtained from the Green's function approach as

$$\mathbf{E}^{(m_\kappa)}(\mathbf{r}) = -\frac{{k_0}^2}{\varepsilon_0}\vec{\mathbf{G}}^{(m_\kappa)}(\mathbf{r},\mathbf{r}')\cdot\delta\vec{\varepsilon}(\mathbf{r}')\cdot\mathbf{E}^{(m_{\kappa'})}(\mathbf{r}') \quad (1)$$

where the indicators κ and $\kappa' = \{0, 1\}$ represent the {TE, TM} polarization and integers m_0 and m_1 label the waveguide modes; $k_0 = 2\pi/\lambda_0$ and ε_0 are the wavenumber and permittivity in vacuum, respectively; $\vec{\mathbf{G}}^{(m_\kappa)}(\mathbf{r},\mathbf{r}')$ is the Green's function corresponding to the m_κth waveguide mode, derived in the previous work,[22] with detailed expressions given in the Appendix; $\delta\vec{\boldsymbol{\varepsilon}}(\mathbf{r}')$ is the dielectric perturbation at the source point; $\mathbf{E}^{(m_{\kappa'})}(\mathbf{r}')$ is the incident guided-wave propagating in the $m_{\kappa'}$th waveguide mode.

In conventional DPLS, two methods were applied to analyze the scattered patterns, termed the correlation method and the amplitude method.[5] The correlation method was used to calculate the integrated scattered optical power from prism-coupled GWDLS, and the derivation relied on the assumption of the simplest ideal grain models.[22] In the present analysis, a Monte Carlo simulation

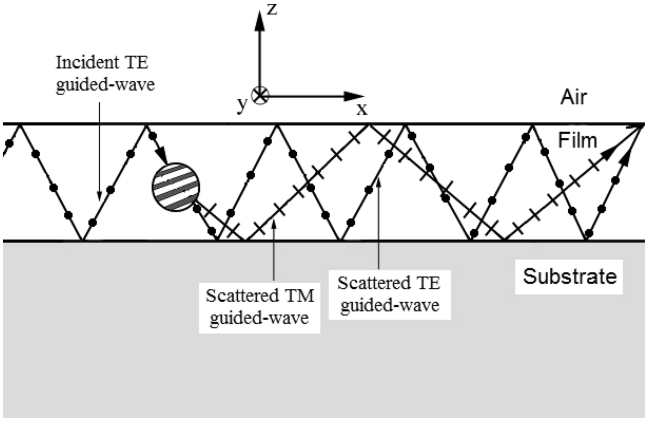

Figure 3. Schematic of the configuration of the waveguide.

based on the amplitude method is used to analyze the angular GWDLS patterns. The scattered intensity at point **r** within the waveguide from source point **r′** is given in the amplitude method as

$$I^{(m_\kappa)}(\mathbf{r}) = \frac{c\varepsilon_0}{2}|\mathbf{E}^{(m_\kappa)}(\mathbf{r})|^2 \quad (2)$$

where c is the velocity of light in a vacuum.

An output coupler creates an "exit" area in the $x-y$ plane, where the guided-wave decays in the total amplitude, while the relative field distribution along the z direction, which is uniquely determined by the waveguide characteristic equation corresponding to the particular waveguide mode,[27] remains unchanged. In other words, the intensity of the outgoing wave from a specific point **r** in the waveguide results from decay of the intensity amplitude at all points with the same transverse position $\boldsymbol{\rho} = (x, y)$ as **r**. Therefore, the intensity at **r** calculated from eq 2 should be normalized to eliminate its z dependence and to obtain the intensity amplitude at corresponding transverse position $\boldsymbol{\rho}$, namely

$$I_N^{(m_\kappa)}(\rho) = \frac{I^{(m_\kappa)}(\mathbf{r})}{N^{(m_\kappa)}(z)} \quad (3)$$

where the normalization coefficients are calculated from

$$N^{(m_0)}(z) = \frac{{E_y}^2(z)d}{\int_{-\infty}^{\infty}{E_y}^2(z)\,\mathrm{d}z}$$

for TE modes and

$$N^{(m_1)}(z) = \frac{{H_y}^2(z)d/{n_2}^2}{\int_{-\infty}^{\infty}[{H_y}^2(z)/n^2(z)]\,\mathrm{d}z}$$

for TM modes; d is the film thickness. Explicit expressions for these coefficients are given in the Appendix.

The illuminated region of a sample in DPLS experiments on bulk samples is bounded by the diameter of the laser beam and the thickness of the sample, both of which are on the order of 1 mm. Under these conditions, the far-field scattered intensity from a grain is independent of the grain's position within the sample; thus, the scattering pattern can be interpreted as the scattered intensity from an "average" grain in the sample multiplied by the number of grains in the total illuminated volume. In thin-film GWDLS experiments, to compensate for the extreme thinness of the sample, the interaction path length has been increased to 1 cm. For a sample with such dimensions, the scattered intensity from a grain depends on its location in the waveguide. Therefore, the Monte Carlo simulation in this analysis explicitly accounts for this position-dependent scattering from grains. The basic idea is depicted in Figure 4, which takes a projected view in the $x-y$ plane. To determine the scattered power at far-field point

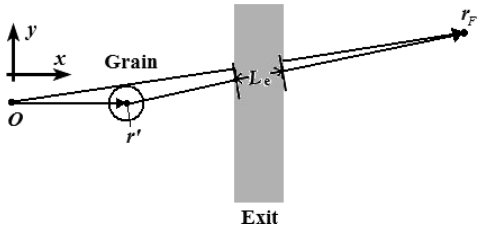

Figure 4. Graphical representation of position-dependent Monte Carlo simulation.

$\mathbf{r}_F$ outside the waveguide contributed by the jth grain which is centered at $\mathbf{r}'$, a path connecting $\boldsymbol{\rho}_F$ and $\boldsymbol{\rho}'$, the transverse components of $\mathbf{r}_F$ and $\mathbf{r}'$, is drawn to find $\mathbf{L}_e$, its intersection with the area covered by the output grating. The contribution from the jth grain is then given by integrating the scattered intensity along this exit path $\mathbf{L}_e$ or

$$I_{Fj}^{(m_\kappa)}(\rho_F) = \frac{1}{L_e}\int_{\mathbf{L}_e} d\mathbf{L}\, I_{Nj}^{(m_\kappa)}(\rho_e) X^{(m_\kappa)}(\rho_e) \tag{4}$$

where the exit factor $X^{(m_\kappa)}(\boldsymbol{\rho}_e)$ denotes the portion of the original intensity amplitude remaining at point $\boldsymbol{\rho}_e$, accounting for the decay of the guided-wave amplitude due to the output coupling, and

$$I_{Nj}^{(m_\kappa)}(\rho_e) = \frac{c\varepsilon_0}{2N^{(m_\kappa)}(z)} |\mathbf{E}_j^{(m_\kappa)}(\mathbf{r}_e)|^2$$
$$= \frac{c\varepsilon_0 k_0{}^4 (n_e{}^2 - n_o{}^2)^2}{2N^{(m_\kappa)}(z)} \left| \int_{V_j} d\mathbf{r}'\, \vec{\mathbf{G}}^{(m_\kappa)}(\mathbf{r}_e, \mathbf{r}') \cdot \left(\hat{\mathbf{g}}_j \hat{\mathbf{g}}_j - \frac{1}{3}\vec{\mathbf{I}} \right) \cdot \mathbf{E}^{(m_{\kappa'})}(\mathbf{r}') \right|^2 \tag{5}$$

where n_e and n_o are the extraordinary and ordinary refractive indices of the grain, respectively, V_j is volume occupied by the jth grain, $\hat{\mathbf{g}}_j$ is the unit vector in the direction of the optic axis of the jth grain, and $\vec{\mathbf{I}}$ is the unit tensor. For computational simplicity, eq 4 can be approximated as

$$I_{Fj}^{(m_\kappa)}(\rho_F) = \frac{\eta_o^{(m_\kappa)}}{L_e}\int_{L_e} d\mathbf{L}\, I_{Nj}^{(m_\kappa)}(\rho_e) \tag{6}$$

where $\eta_o^{(m_\kappa)}$ is the output efficiency of the m_κth guided wave, which can be calculated from the grating parameters and the waveguide mode information using the Green's function approach.[24] For the pattern shown in Figure 2, $\eta_o^{(m_0)} = 0.961$ and $\eta_o^{(m_1)} = 0.521$.

The position-dependent scattering method employed in eqs 4 and 5 assumes that all outgoing waves scattered from the jth grain exit along $\boldsymbol{L}_e$, which is reasonable when the separation between points $\boldsymbol{\rho}_F$ and $\boldsymbol{\rho}'$ is much greater than the grain size. When the interference terms between different grains are assumed to be zero, the contribution from each independent grain can then be added up incoherently. In the Monte Carlo simulation, a collection of identical grains is generated with random positions and orientations, and their scattering contributions are added up to obtain the scattered pattern observed at the screen as

$$I_F^{(m_\kappa)}(\rho_F) = \frac{V}{\sum_j V_j}\sum_j I_{Fj}^{(m_\kappa)}(\rho_F) \tag{7}$$

where V is the total illuminated volume. The distance between the output grating and the screen is chosen to be 20 cm in the Monte Carlo simulation in order to match the experimental conditions.

The correlation method used in the previous work was limited to ideal grain models, whereas the Monte Carlo simulation using the amplitude method allows more complicated grain models, such as the ellipsoidal grain model, which was generally assumed in bulk DPLS, as shown in Figure 5. The randomly generated grains in the simulation can partly exceed the film boundaries,

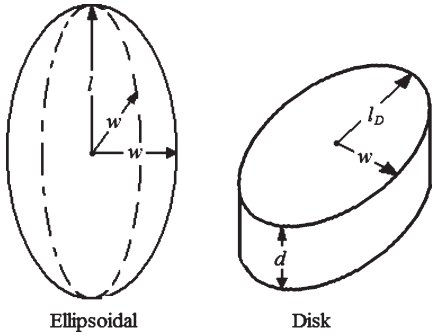

Figure 5. Ellipsoidal and disk grain models.

and their shapes should be cut off accordingly. When the grain sizes are assumed to be comparable to or even greater than the film thickness, this cutoff effect can be significant. In this extreme, it is reasonable to truncate the ellipsoids to define a more realistic "disk" model, as also depicted in Figure 5. The major axis of the ellipse cross section of the disk, l_D, ranges from w to l depending on the polar angle θ_D of the optic axis, given by

$$l_D = \sqrt{l^2 \sin^2\theta_D + w^2 \cos^2\theta_D} \tag{8}$$

Fitting Procedure

The observed GWDLS pattern contains the contributions from both the grains and the grating birefringence. In order to separate these two components to obtain structural information on the grains, the measured angular pattern should be fitted with an expression that takes both depolarization components into account, i.e.

$$I_{DP}(\psi) = I_{DP}^{Grains}(\psi; l, w) + I_{DP}^{Grating}(\psi; \Delta n_{grating}) \tag{9}$$

where ψ is the scattering angle, $I_{DP}^{Grain}(\psi)$ and $I_{DP}^{Grating}(\psi)$ denote the depolarization contribution from the grains and the gratings, respectively, and the parameters l, w, and $\Delta n_{grating}$ are fitted to the experimental scattering data.

Among the two sources of the depolarization, the grain contribution $I_{DP}^{Grain}(\psi)$ can be calculated using the Monte Carlo simulation method described in the previous section. The far-field vector $\boldsymbol{\rho}_F$ is converted to the scattering angle ψ via $\psi = \arctan(y_F/x_F)$.

Attention needs to be paid to the depolarization from the gratings. In the previous work, it was found that the grating contribution is given by

$$I_{DP}^{Grating}(\psi) = A \sin^2 2\psi I_P(\psi) \tag{10}$$

where $I_P(\psi)$ is the polarized scattered intensity exiting the waveguide through the output grating coupler and A is the birefringence amplitude factor given by

$$A = \left(\frac{\pi \Delta n_{grating} l_p}{\lambda}\right)^2 \cos^4\theta_i \tag{11}$$

where $\Delta n_{grating}$ is the birefringence of the grating, l_p is the interaction path length of the light with the output grating, and θ_i is the angle between the direction of propagation of light inside the substrate and a normal to the substrate surface.

The expression for $I_{DP}^{Grating}(\psi)$ in eq 10 is based on the far-field approximation. As previously mentioned, the derivation of $I_{DP}^{Grain}(\psi)$ is based on the position-dependent Monte Carlo method. Therefore, when fitting the measured GWDLS pattern with eq 9, using eq 10 to calculate depolarization from the gratings is internally inconsistent. In order to calculate $I_{DP}^{Grating}(\psi)$ consistently with $I_{DP}^{Grain}(\psi)$, a similar Monte Carlo simulation method is employed. The source points are randomly assigned in the waveguide, and each source point is set as the new origin to calculate the

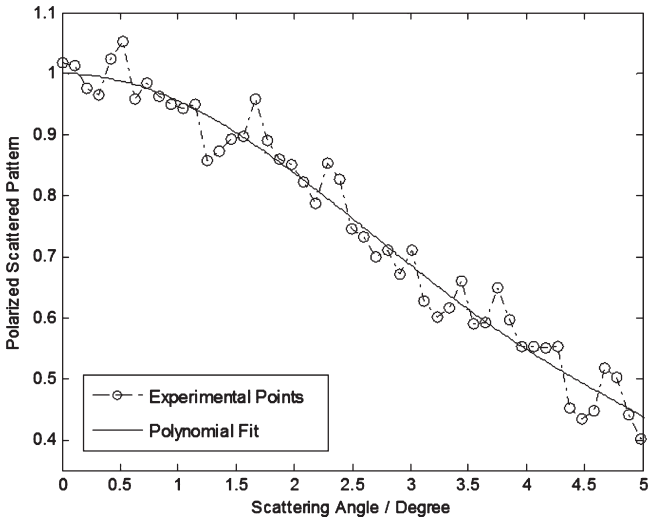

Figure 6. Experimental polarized scattering pattern and the polynomial fit, normalized to unity at zero scattering angle. Uncertainties are ±5%.

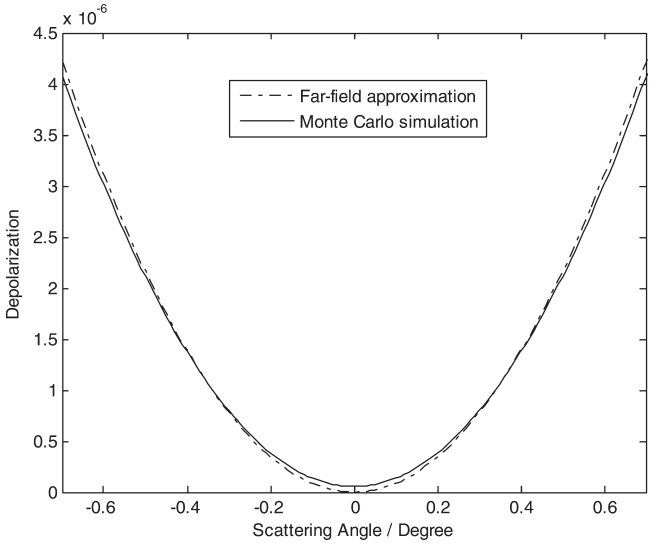

Figure 7. Grating birefringence signal calculated using different methods, normalized as in Figure 6. Uncertainties are ±5%.

scattering angle for each observation point. Equation 10 is then used to calculate the grating depolarization using the newly defined scattering angles, and $I_{DP}^{Grating}(\psi)$ is obtained by averaging the contributions from all randomly generated source points, namely

$$I_{DP}^{Grating}(\psi) = \frac{1}{N}\sum_{j=1}^{N}[I_P(\psi_j)A\sin^2 2\psi_j] \qquad (12)$$

where N is the number of the random source points, ψ_j is the scattering angle redefined for the jth source point, and $I_P(\psi_j)$ is the angular intensity distribution of the incident polarized wave normalized with respect to $I_P(0)$. The factor $I_P(\psi_j)$ replaces $I_P(\psi)$ because in the Monte Carlo simulation method the angular distribution of the polarized intensity is needed for each randomly assigned source point since the scattering angles are redefined and are thus different for each point. The local distribution of $I_P(\psi_j)$ results from scattering from both the grains and the surface imperfections of the waveguide and cannot be quantitatively modeled. As a practical approximation, we use a polynomial fitted to the measured angular pattern of the scattered polarized light, denoted as $I_P^{Exp}(\psi)$, as an approximation of $I_P(\psi_j)$ for all source points. The polynomial fit is shown in Figure 6.

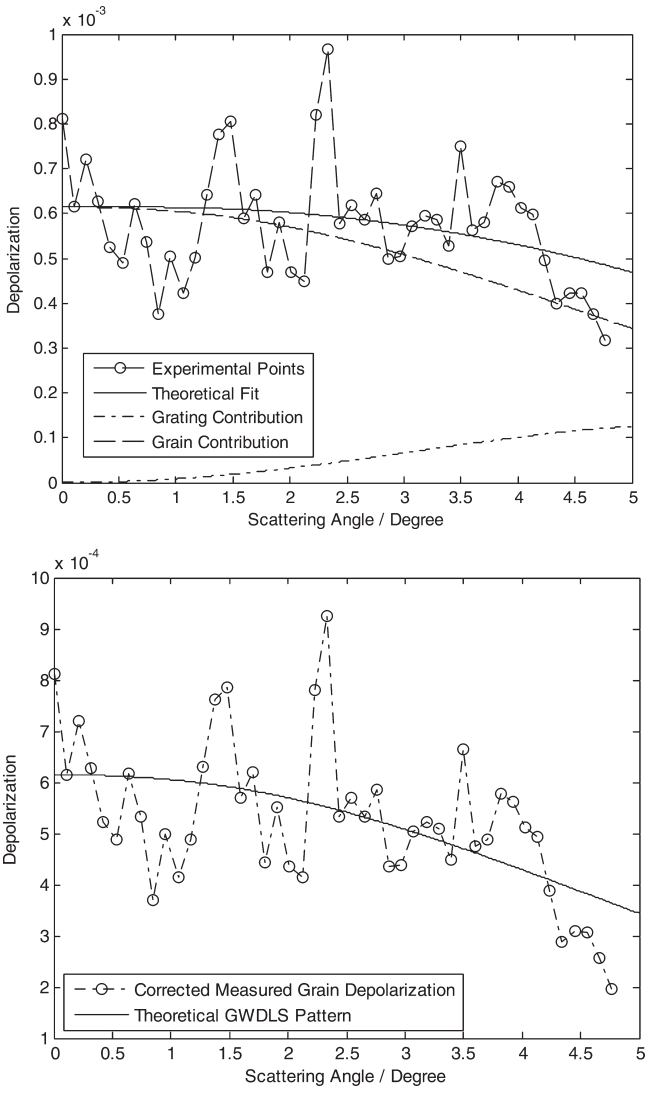

Figure 8. Fitting of the measured GWDLS pattern. (top) Fitting the total experimental depolarized pattern, normalized as in Figure 6; the solid line is the sum of the grating and grain contributions. (bottom) Depolarized pattern after subtracting the grating contribution. Uncertainties are ±10%.

The grating birefringence calculated using these two methods is compared in Figure 7. The grating birefringence calculated based on the far-field approximation is lower at very small scattering angles and higher at larger angles compared to that obtained using the Monte Carlo simulation, although for our experimental data, the difference between the curves is not significant. Use of the far-field method could cause errors in cases where the grating birefringence is larger.

The depolarized angular pattern shown in Figure 2 was fitted to eqs 9 and 10, and the result is shown in Figure 8. A similar pattern was obtained from the second film/grating combination. The spikes seen are due to speckle in the measured pattern which results from interference of scattered light from different grains. The best-fit grain model is a disk model with $w = 0.4 \pm 0.1\ \mu$m and $l = 2.8 \pm 0.7\ \mu$m. Analysis of the pattern from the second film yielded comparable grain parameters. This large grain size is consistent with the disk model, which indicates the cutoff effect of the grains by the thin-film boundaries. The depolarized contribution from the grating is considerably smaller than that from the grains, demonstrating that an optimally designed grating coupler can effectively reduce the grating birefringence signal. This is consistent with the small $\Delta n_{grating}$ value, determined from the fit to be

0.055 ± 0.009, which is close to the theoretical value assuming that the grooves are filled with air (0.085) while much lower than the one reported in the previous work (0.155).[23]

Concluding Remarks

We have demonstrated that angular scattered patterns from grating-coupled guided-wave depolarized light scattering can be analyzed to obtain detailed structural information on the block copolymer thin films. The measured pattern consists of depolarization contributions from both the ordered grains and the birefringent grating coupler, which can be separated through a three-parameter (l, w, and $\Delta n_{\text{grating}}$) least-squares fitting procedure. A suitable grain model for the thin-film samples is found to be disks lying in the film plane with elliptical cross section, randomly oriented optic axes, and variable-length major axes, which is different from the ellipsoidal grain model more commonly used for bulk samples and indicates a cutoff effect of the lateral confinement in thin-film samples. Using the methods developed in this paper, more details of the disk-forming dynamics can be expected from temperature-scan measurements of the angular GWDLS patterns. The method is limited to block copolymer microphases that exhibit form birefringence, namely lamellar and cylindrical microphases, and a good optical contrast (i.e., refractive index difference) between the two microdomains is required. Although the reported signals are quite weak, this technique could be applied to the study of polymer films thinner than 500 nm. In our present air/film/substrate geometry, and for film and substrate with refractive indices of 1.54 (SI(7−23)) and 1.46 (fused silica), respectively, the film must be at least 285 nm thick to support one TE and one TM mode. The expected weaker scattering could be offset by using higher-power laser sources. To study even thinner samples, one must employ a symmetric substrate/film/substrate geometry, in which the polymer film is sandwiched between two silica substrates.[27] Although there is still room for improvements in the technique, the grating-coupled GWDLS can now perform most functions of the traditional DPLS under the theoretical and experimental framework developed in this paper.

Acknowledgment. Financial support provided by the National Science Foundation (Grants DMR-0514422, DMR-0966662, and DMR-0966765) is gratefully acknowledged. We thank Ming Leung for helpful discussions in the numerical computations, Amish Patel for synthesizing the polymer samples, and Jeffrey Wilbur for his effort in the development of the GWDLS technique.

Appendix

Components of the Green's function dyadic corresponding to each waveguide mode take the form

$$g_{\alpha\beta}^{(m_k)}(k_\rho^{(m_k)};\mathbf{r},\mathbf{r}') = c_{\alpha\beta}^{(m_k)}(k_\rho^{(m_k)};\rho_s)\,l^{(m_k)}(k_\rho^{(m_k)};z,z') \qquad (A.1)$$

where $\boldsymbol{\rho}_s = (x - x', y - y') = (\rho_s, \phi_s)$ is the transverse separation vector. The common factors are

$$l^{(m_0)}(k_\rho^{(m_0)};z,z') = \frac{ik_{2z}^{(m_0)}|k_{1z}^{(m_0)}k_{3z}^{(m_0)}|\cos\left[k_{2z}^{(m_0)}z+\frac{\Theta^{(m_0)}}{2}\right]\cos\left[k_{2z}^{(m_0)}z'+\frac{\Theta^{(m_0)}}{2}\right]}{k_\rho^{(m_0)}[|k_{1z}^{(m_0)}|+|k_{3z}^{(m_0)}|+|k_{1z}^{(m_0)}k_{3z}^{(m_0)}|d]}$$

$$l^{(m_1)}(k_\rho^{(m_1)};z,z') = \frac{-k_{1z}^{(m_1)}k_{2z}^{(m_1)}k_{3z}^{(m_1)}\cos\left[k_{2z}^{(m_1)}z+\frac{\Theta^{(m_1)}}{2}\right]\sin\left[k_{2z}^{(m_1)}z'+\frac{\Theta^{(m_1)}}{2}\right]}{k_\rho^{(m_1)}[K_3^{(m_1)}|k_{1z}^{(m_1)}|+K_1^{(m_1)}|k_{3z}^{(m_1)}|-k_{1z}^{(m_1)}k_{3z}^{(m_1)}d]} \qquad (A.2)$$

where

$$k_\rho^{(m_k)} = k_2 \sin\theta_g^{(m_k)}$$

$$k_i^{(m_k)} = \sqrt{k_i^{\,2} - [k_\rho^{(m_k)}]^2}, \quad i = 1, 2, 3$$

$$\Theta^{(m_0)} = \arccos\left\{\frac{[k_{2z}^{(m_0)}]^2 - |k_{3z}^{(m_0)}|^2}{[k_{2z}^{(m_0)}]^2 + |k_{3z}^{(m_0)}|^2}\right\}$$

$$\Theta^{(m_1)} = \arccos\left\{\frac{[k_{2z}^{(m_1)}]^2 - |\overline{k}_{1z}^{(m_1)}|^2}{[k_{2z}^{(m_1)}]^2 + |\overline{k}_{1z}^{(m_1)}|^2}\right\}$$

$$K_i^{(m_1)} = \frac{[k_{2z}^{(m_1)}]^2 + |k_{iz}^{(m_1)}|^2}{(n_i/n_2)^2[k_{2z}^{(m_1)}]^2 + |\overline{k}_{iz}^{(m_1)}|^2}$$

and $\overline{k}_{iz}^{(m_1)} = n_2^{\,2}k_{iz}^{(m_1)}/n_i^2$, $i = 1$ or 3. And the component-specific factors are

$$c_{xx}^{(m_0)}(k_\rho^{(m_0)};\rho_s) = \frac{1}{k_{2z}^{(m_0)}}\left[k_\rho^{(m_0)}J_0(k_\rho^{(m_0)}\rho_s)\sin^2\phi_s + \frac{1}{\rho_s}J_1(k_\rho^{(m_0)}\rho_s)\cos(2\phi_s)\right]$$

$$c_{xy}^{(m_0)}(k_\rho^{(m_0)};\rho_s) = c_{yx}^{(m_0)}(k_\rho^{(m_0)};\rho_s) = \frac{1}{k_{2z}^{(m_0)}}\left[-k_\rho^{(m_0)}J_0(k_\rho^{(m_0)}\rho_s) + \frac{2}{\rho_s}J_1(k_\rho^{(m_0)}\rho_s)\right]\sin\phi_s\cos\phi_s$$

$$c_{yy}^{(m_0)}(k_\rho^{(m_0)};\rho_s) = \frac{1}{k_{2z}^{(m_0)}}\left[k_\rho^{(m_0)}J_0(k_\rho^{(m_0)}\rho_s)\cos^2\phi_s - \frac{1}{\rho_s}J_1(k_\rho^{(m_0)}\rho_s)\cos(2\phi_s)\right]$$

$$c_{xz}^{(m_0)}(k_\rho^{(m_0)};\rho_s) = c_{zx}^{(m_0)}(k_\rho^{(m_0)};\rho_s) = c_{yz}^{(m_0)}(k_\rho^{(m_0)};\rho_s) = c_{zy}^{(m_0)}(k_\rho^{(m_0)};\rho_s) = c_{zz}^{(m_0)}(k_\rho^{(m_0)};\rho_s) = 0 \qquad (A.3)$$

and

$$c_{xx}^{(m_1)}(k_\rho^{(m_1)};\rho_s) = \frac{k_{2z}^{(m_1)}}{k_2^{\,2}}\left[k_\rho^{(m_1)}J_0(k_\rho^{(m_1)}\rho_s)\cos^2\phi_s - \frac{1}{\rho_s}J_1(k_\rho^{(m_1)}\rho_s)\cos(2\phi_s)\right]$$

$$c_{xy}^{(m_1)}(k_\rho^{(m_1)};\rho_s) = c_{yx}^{(m_1)}(k_\rho^{(m_1)};\rho_s) = \frac{k_{2z}^{(m_1)}}{k_2^{\,2}}\left[k_\rho^{(m_1)}J_0(k_\rho^{(m_1)}\rho_s) - \frac{2}{\rho_s}J_1(k_\rho^{(m_1)}\rho_s)\right]\sin\phi_s\cos\phi_s$$

$$c_{xz}^{(m_1)}(k_\rho^{(m_1)};\rho_s) = c_{zx}^{(m_1)}(k_\rho^{(m_1)};\rho_s) = -\frac{i[k_\rho^{(m_1)}]^2}{k_2^{\,2}}J_1(k_\rho^{(m_1)}\rho_s)\cos\phi_s$$

$$c_{yy}^{(m_1)}(k_\rho^{(m_1)};\rho_s) = \frac{k_{2z}^{(m_1)}}{k_2^{\,2}}\left[k_\rho^{(m_1)}J_0(k_\rho^{(m_1)}\rho_s)\sin^2\phi_s + \frac{1}{\rho_s}J_1(k_\rho^{(m_1)}\rho_s)\cos(2\phi_s)\right]$$

$$c_{yz}^{(m_1)}(k_\rho^{(m_1)};\rho_s) = c_{zy}^{(m_1)}(k_\rho^{(m_1)};\rho_s) = -\frac{i[k_\rho^{(m_1)}]^2}{k_2^2}J_1(k_\rho^{(m_1)}\rho_s)\sin\phi_s$$

$$c_{zz}^{(m_1)}(k_\rho^{(m_1)};\rho_s) = \frac{[k_\rho^{(m_1)}]^3}{k_2^{\,2}k_{2z}^{(m_1)}}J_0(k_\rho^{(m_1)}\rho_s) \qquad (A.4)$$

The scaling coefficients in eq 3 are

$$N^{(m_0)}(z) = \frac{2[k_{2z}^{(m_0)}]^2\left\{\cos[k_{2z}^{(m_0)}z] - \frac{|k_{3z}^{(m_0)}|}{k_{2z}^{(m_0)}}\sin[k_{2z}^{(m_0)}z]\right\}^2}{\{[k_{2z}^{(m_0)}]^2 + |k_{3z}^{(m_0)}|^2\}\left[d + \frac{1}{|k_{1z}^{(m_0)}|} + \frac{1}{|k_{3z}^{(m_0)}|}\right]}$$

$$N^{(m_1)}(z) = \frac{2|\overline{k}_{3z}^{(m_1)}|^2\left\{-\frac{k_{2z}^{(m_1)}}{|\overline{k}_{3z}^{(m_1)}|}\cos[k_{2z}^{(m_1)}z] + \sin[k_{2z}^{(m_1)}z]\right\}^2}{\{[k_{2z}^{(m_1)}]^2 + |\overline{k}_{3z}^{(m_1)}|^2\}\left\{d + \frac{[k_{2z}^{(m_1)}]^2 + |k_{1z}^{(m_1)}|^2}{[k_{2z}^{(m_1)}]^2 + |\overline{k}_{1z}^{(m_1)}|^2}\frac{n_2^2}{n_1^2|k_{1z}^{(m_1)}|} + \frac{[k_{2z}^{(m_1)}]^2 + |k_{3z}^{(m_1)}|^2}{[k_{2z}^{(m_1)}]^2 + |\overline{k}_{3z}^{(m_1)}|^2}\frac{n_2^2}{n_3^2|k_{3z}^{(m_1)}|}\right\}} \quad \text{(A.5)}$$

References and Notes

(1) Bates, F. S.; Fredrickson, G. H. *Annu. Rev. Phys. Chem.* **1990**, *41*, 525.
(2) Hadjichristidis, N.; Pispas, S.; Floudas, G. *Block Copolymer*; Wiley-Interscience: New York, 2003; Chapter 17.
(3) Balsara, N. P.; Garetz, B. A.; Dai, H. J. *Macromolecules* **1992**, *25*, 6072.
(4) Floudas, G.; Fytas, G.; Hadjichristidis, N.; Pitsikalis, M. *Macromolecules* **1995**, *28*, 2359.
(5) Newstein, M. C.; Garetz, B. A.; Balsara, N. P.; Chang, M. Y.; Dai, H. J. *Macromolecules* **1998**, *31*, 64.
(6) Wang, H.; Newstein, M. C.; Chang, M. Y.; Balsara, N. P.; Garetz, B. A. *Macromolecules* **2000**, *33*, 3719.
(7) Chastek, T. Q.; Lodge, T. P. *Macromolecules* **2003**, *36*, 7672.
(8) Chastek, T. Q.; Lodge, T. P. *Macromolecules* **2004**, *37*, 4891.
(9) Chastek, T. Q.; Lodge, T. P. *J. Polym. Sci., Part B: Polym. Phys.* **2005**, *43*, 405.
(10) Park, M.; Harrison, C.; Chaikin, P. M.; Register, R. A.; Adamson, D. H. *Science* **1997**, *276*, 1401.
(11) Mansky, P.; Liu, Y.; Huang, E.; Russell, T. P.; Hawker, C. *Science* **1997**, *275*, 1458.
(12) Cheng, J. Y.; Ross, C. A.; Thomas, E. L.; Smith, H. I.; Vancso, G. J. *Appl. Phys. Lett.* **2002**, *81*, 3657.
(13) Lau, K. H. A.; Bang, J.; Kim, D. H.; Knoll, W. *Adv. Funct. Mater.* **2008**, *18*, 3148.
(14) Messerschmidt, M.; Millaruelo, M.; Choinska, R.; Jehnichen, D.; Voit, B. *Macromolecules* **2009**, *42*, 156.
(15) Sivaniah, E.; Hayashi, Y.; Matsubara, S.; Kiyono, S.; Hashimoto, T.; Fukunaga, K.; Kramer, E. J.; Mates, T. *Macromolecules* **2005**, *38*, 1837.
(16) Tsarkova, L.; Horvat, A.; Krausch, G.; Zvelindovsky, A. V.; Sevink, G. J. A.; Magerle, R. *Langmuir* **2006**, *22*, 8089.
(17) Müller-Buschbaum, P.; Casagrande, M.; Gutmann, J.; Kuhlmann, T.; Stamm, M.; von Krosigk, G.; Lode, U.; Cunis, S.; Gehrke, R. *Europhys. Lett.* **1998**, *42*, 517.
(18) Yoon, J.; Jin, S.; Ahn, B.; Rho, Y.; Hirai, T.; Maeda, R.; Hayakawa, T.; Kim, J.; Kim, K.; Ree, M. *Macromolecules* **2008**, *41*, 8778.
(19) Virgili, J. M.; Tao, Y.; Kortright, J. B.; Balsara, N. P.; Segalman, R. A. *Macromolecules* **2007**, *40*, 2092.
(20) Müller-Buschbaum, P.; Cubitt, R.; Petry, W. *Langmuir* **2003**, *19*, 7778.
(21) Garetz, B. A.; Newstein, M. C.; Wilbur, J. D.; Patel, A. J.; Durkee, D. A.; Segalman, R. A.; Liddle, J. A.; Balsara, N. P. *Macromolecules* **2005**, *38*, 4282.
(22) Fang, Z.; Newstein, M. C.; Garetz, B. A.; Wilbur, J. D.; Balsara, N. P. *J. Opt. Soc. Am. B* **2007**, *24*, 1291.
(23) Wilbur, J. D.; Fang, Z.; Garetz, B. A.; Newstein, M. C.; Balsara, N. P. *Macromolecules* **2008**, *41*, 4464.
(24) Fang, Z. Ph.D. Dissertation, Polytechnic Institute of NYU, Brooklyn, NY, June 2009.
(25) Giallorenzi, T. G.; Sheridan, J. P. *J. Appl. Phys.* **1975**, *46*, 1271.
(26) Abuzaina, F. M.; Garetz, B. A.; Patel, A. J.; Newstein, M. C.; Gido, S. P.; Hu, X.; Balsara, N. P. *Macromolecules* **2006**, *39*, 3377.
(27) Yariv, A.; Yeh, P. *Optical Waves in Crystals: Propagation and Control of Laser Radiation*; John Wiley & Sons, Inc.: New York, 1984.